Dalton Transactions

K3LaTe2O9: a New Alkali-Rare Earth Tellurate with Face-Sharing TeO6 Octahedra

Journal:	*Dalton Transactions*
Manuscript ID:	DT-ART-06-2015-002255.R1
Article Type:	Paper
Date Submitted by the Author:	18-Jul-2015
Complete List of Authors:	Zhang, Xinyuan; Technical Institute of Physics and Chemistry, CAS, ; University of Chinese Academy of SciencesUniversity of Chinese Academy of Sciences, Yao, Jiyong; Technical Institute of Physics and Chemistry, Jiang, Xingxing; Beijing Center for Crystal R&D, Key Lab of Functional Crystals and Laser Technology of Chinese Academy of Sciences, Technical Institute of Physics and Chemistry, Chinese Academy of Sciences, ; University of Chinese Academy of Sciences, Fu, Ying; Technical Institute of Physics and Chemistry, ; University of Chinese Academy of Sciences, Lin, Zheshuai; Technical Institute of Physics and Chemistry, Chinese Academy of Sciences, Zhang, Guochun; Technical Institute of Physics and Chemistry, ; Wu, Yicheng; Technical Institute of Physics and Chemistry, Chinese Academy of Sciences,

Highlight

$K_3LaTe_2O_9$, a rare quaternary alkali-lanthanide tellurate with face-sharing TeO_6 octahedra.

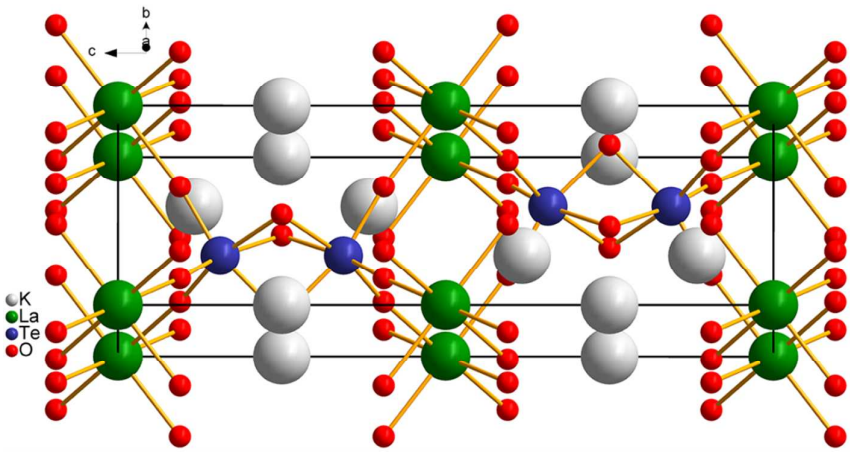

$K_3LaTe_2O_9$: a New Alkali-Rare Earth Tellurate with Face-Sharing TeO_6 Octahedra †

Xinyuan Zhang,[a,b] Jiyong Yao,[a] Xingxing Jiang,[a,b] Ying Fu,[a,b] Zheshuai Lin,[a] Guochun Zhang,[*a] and Yicheng Wu[a]

[a]*Beijing Center for Crystal Research and Development, Key Laboratory of Functional Crystals and Laser Technology, Technical Institute of Physics and Chemistry, Chinese Academy of Sciences, Beijing 100190, P. R. China. Email: gczhang@mail.ipc.ac.cn*

[b]*University of Chinese Academy of Sciences, Beijing 100049, P. R. China*

† Electronic Supplementary Information (ESI) available: Crystallographic data in CIF format for CCDC 1406510

Abstract:

A new quaternary alkali-lanthanide metal tellurate $K_3LaTe_2O_9$ has been synthesized by conventional high-temperature solid state method, and single crystals have been grown by spontaneous crystallization. $K_3LaTe_2O_9$ crystallizes in hexagonal space group $P6_3/mmc$, with $a = b = 6.0589(9)$ Å, $c = 15.024(3)$ Å, and Z = 2. In the structure, $[Te_2O_9]^{6-}$ contains rare face-sharing TeO_6 polyhedra, which are connected by LaO_6 octahedra forming a three-dimensional framework structure. Furthermore, its properties are investigated by UV-vis-NIR diffuse reflectance spectroscopy, Raman and IR spectra, thermal analysis, variable-temperature X-ray powder diffraction, and first- principles calculations.

Introduction

Tellurates have attracted much attention because of their rich structural chemistry

and interesting physical properties, such as nonlinear optical (NLO) properties, ferroelectric properties, and magnetic properties, etc. [1-4] Generally, the Te stereochemistry plays an important role in determining overall atomic and electronic structure and physical properties. [5-8] For instance, in BaMTe^{IV}Te^{VI}O$_7$ (M = Mg^{2+} or Zn^{2+}), Te^{VI}O$_6$ octahedra link with asymmetric Te^{IV}O$_4$ polyhedra to make a continuous layer with polar symmetry, leading to moderate second harmonic generating capability.[1] A_2CoTeO$_6$ perovskites (A = Cd, Ca, Sr, Pb, and Ba) are antiferromagnetic at low temperatures, and the unique decrease in antiferromagnetic interaction show that Te^{6+} cations affect the electronic and the magnetic structure in the compounds, which is not observed in A_2^{2+}CoM^{6+}O$_6$ with other similar ionic sizes of M^{6+}.[2]

Up to now, quaternary alkali-rare earth metal tellurate compounds have been seldom reported besides polycrystalline Eu^{3+}-doped Li$_3$Y$_3$Te$_2$O$_{12}$.[9] Since La has the d^0 electronic configuration, which can induce distortion of coordination polyhedra through a second-order Jahn-Teller effect[10] leading to interesting structures and properties, many efforts were made to synthesize new A/La/TeO compouds. For example, A$_2$(BB')O$_6$ perovskite compounds MLaMgTeO$_6$ (M = Na, K) show layer-like ordering of alkali and La^{3+} ions in A sites, with strong distortion of MgO$_6$ and TeO$_6$ octahedra.[11]

In order to search for novel structures or new functional materials, we investigated further the alkali-rare earth tellurate systems, which led us to find K$_3$LaTe$_2$O$_9$, a rare quaternary alkali-lanthanide tellurate, with only the second refined structure after Ba$_3$Te$_2$O$_9$[11, 12] in which TeO$_6$ octahedra share faces rather than edges or corners. In

this work, we present the growth, structure, optical and thermal properties of $K_3LaTe_2O_9$ crystal.

Experimental section

Synthesis and Growth

Polycrystalline samples of $K_3LaTe_2O_9$ were prepared by solid-state reaction. The initial reactants were K_2CO_3, La_2O_3, and H_6TeO_6 (all analytically pure). Before weighing, La_2O_3 was pre-heated at 600 ℃ for 12 h to remove H_2O. A mixture of K_2CO_3, La_2O_3, and H_6TeO_6 in the molar ratio of 3: 1: 4 was ground and preheated in an Al_2O_3 crucible at 400℃ in air for 10 h to decompose the carbonate and eliminate the water. The products were cooled to room temperature and ground. Then the products were heated to 650℃ and held for three days with several intermediate grindings until single-phase powders were obtained.

X-ray powder diffraction analysis of the polycrystalline samples was performed at room temperature using an automated Bruker D8 X-ray diffractometer equipped with a diffracted monochromator set for Cu Kα (λ = 1.5418 Å) radiation. A scanning step width of 0.02 º and the scanning rate of 0.1 s/step were applied to record the pattern in the 2θ range of 10- 70 º. The XRD pattern of $K_3LaTe_2O_9$ powder was in good agreement with the calculated pattern on the basis of the single crystal crystallographic data of $K_3LaTe_2O_9$ (Figure 1).

Single crystals of $K_3LaTe_2O_9$ were grown by spontaneous crystallization. A mixture of K_2CO_3, La_2O_3, and H_6TeO_6 in the molar ratio of 3: 1: 6 was ground in an agate mortar and melted into a platinum crucible in several batches. The crucible was

placed in a programmable temperature furnace, heated to 650 °C in air, and held for 10 h, then slowly cooled to 200°C at a rate of 3- 4 °C h^{-1} followed by rapid cooling to room temperature. The product consisted of colorless crystals, which were manually selected for structure characterization. EDX analysis was carried out on a Hitachi S-4800 SEM, which showed that the approximate molar ratio of K, La, and Te is 3: 1: 2. ICP-AES was carried out on a IRIS Intrepid II XSP, which showed that the molar ratio of K, La, and Te is 3.2 : 1: 2.3.

Structure Determination

Single-crystal X-ray diffraction data at 293 K were collected on a Rigaku AFC10 diffractometer (Mo Kα, λ = 0.71073 Å) equipped with a Saturn CCD detector. Crystal decay was monitored by re-collecting 50 initial frames at the end of data collection. The collection of the intensity data, cell refinement, and data reduction were carried out with the program Crystalclear.[13] Face-indexed absorption corrections were performed numerically by using the program XPREP.[14]

The structure was solved with the direct methods program SHELXS and refined with the least-squares program SHELXL of the SHELXTL.PC suite of programs.[14] The final refinement included anisotropic displacement parameters and a secondary extinction correction. The program STRUCTURE TIDY[15] was then employed to standardize the atomic coordinates. Additional details and structural data are given in Tables 1-3, and further information can be found in Supplementary information.

First-principles calculations

The first-principles studies on the electronic density difference and Mulliken

atomic/bond populations[16] were performed by the plane-wave pseudopotential method[17] implemented in the CASTEP package[18] based on density functional theory (DFT).[19] The functional[20] developed by Ceperley, Alder Perdew, and Zunger (CA-PZ) in local density approximation (LDA) form were adopted to search the minimum of the electron energy. The optimized norm-conserving pseudopentials[21] in Kleiman-Bylander form[22] allow us to use a small plane basis set without compromising the accuracy required by the calculation. Kinetic energy cutoff of 900 eV and Monkhorst-pack k-point mesh spanning less than 0.03 $Å^{-1}$ in the Brillouin zone were chosen.[23]

Spectroscopic Characterization

A Cary 5000 UV–vis–NIR spectrophotometer with a diffuse reflectance accessory was used to measure the diffuse reflectance spectrum of $K_3LaTe_2O_9$ in the range of 200 to 2500 nm. The mid-infrared spectrum in a range from 400 to 1200 cm^{-1} at room temperature was obtained by a Bio-Rad FTS-60 FTIR spectrometer with resolution of 1 cm^{-1}. The Raman pattern from 100 to 1200 cm^{-1} at room temperature was recorded on Via-Reflex equipped with a 532 nm solid state laser.

Thermal analysis

A LabsysTM TG-DTA16 (SETARAM) thermal analyzer was used to investigate the thermal property by differential scanning calorimetric (DSC) analysis. About 10 mg $K_3LaTe_2O_9$ samples were placed in an Al_2O_3 crucible, heated at a rate of 10 ℃ min^{-1} from room temperature to 900 ℃ and then cooled to room temperature at the same rate. The thermal gravimetric analysis (TGA) in nitrogen was performed on a

Perkin-Elmer Diamond TG/DTA spectrometer, and heating rate was about 10 °C min^{-1}.

Variable-temperature X-ray powder diffraction (VT-XRD)

The variable-temperature X-ray powder diffraction was recorded on a Bruker D8-discover X-ray diffractometer equipped with a diffracted monochromator set for Cu Kα (λ = 1.5418 Å). Patterns at high temperature (298-1123K) were separately recorded with scanning step width of 0.01°. The high-temperature condition was obtained by an Anton Paar HTK 1200N high-temperature oven.

Results and Discussion

Crystal Structure

As seen in Figure 2, $K_3LaTe_2O_9$ compound crystallizes in centrosymmetric hexagonal space group *P6₃/mmc*. There are two crystallographically independent K atoms, one independent La atom, one independent Te atom, and two independent O atoms in the symmetry unit. K1, K2, La1, Te1, O1, and O2 atoms are in the Wyckoff sites 2b, 4f, 2a, 4f, 6h, and 12k, respectively. The occupancy of all sites is 100%. The oxidation state of 1+, 3+, 6+, and 2- can be assigned to K, La, Te, and O atoms, respectively.

The coordination environments of the cations in $K_3LaTe_2O_9$ are shown in Figure 3. In its structure, Te1 atoms are coordinated to six O atoms to form distorted octahedra. Te-O bonds lengths are respectively 1.860(3) Å for O(2) atoms, which share corners with LaO_6 octahedra, and 2.016(3) Å for O(1), which form the face shared by two TeO_6 octahedra, similar to that of $Ag_2Te_2O_6$ (1.8635 Å to 2.0420 Å)

and $Ba_3Te_2O_9$ (1.8455 Å to 1.9925 Å).[12, 24] The Te1-O-Te1 angles in $[Te_2O_9]^{6-}$ anions are almost 89.00(15)°, resembling $Ba_3Te_2O_9$ (89.720°) in a similar coordination environment. Since each TeO_6 is linked to only one other, these octahedra form isolated face-sharing dimeric anions, $[Te_2O_9]^{6-}$. Meanwhile, La atoms are linked to six O atoms in regular octahedra with the La-O bond lengths of 2.358(3) Å. The La-O-Te angles are 172.71(16) °, comparable to those in the similar coordination environment of (Fe)2a–O2–(Fe/Te)4f in $Ba_3Fe_2TeO_9$ (175.3(1)°).[3] K1 atoms are surrounded by twelve O atoms to form distorted cuboctahedra with K-O bond lengths from 3.000(3) Å to 3.0505(18) Å, and K2 atoms are surrounded by nine O atoms to form distorted octahedra with K-O bond lengths from 2.875(3) Å to 3.051(4) Å. The terminal oxygen atoms in $[Te_2O_9]^{6-}$ anions are linked by sharing corner with LaO_6 octahedron and build a three-dimensional framework structure. K^+ cations occupied the interstices surrounded by Te-O polyhedra and La-O polyhedra, as seen in Figure 4.

According to Pauling's third and fourth rules, repulsion between high-charge cations means that polyhedra containing them are most stable if they share corners, less stable if they share edges and even less so if they share faces.[25, 26] Thus, corner-sharing pattern is the most common way to connect polyhedra in inorganic compounds, such as borates, silicates, phosphates, and tellurates.[27-30] The edge- or face-sharing patterns are rarely found in the above compounds except under extreme conditions, for instance, $Dy_4B_6O_{15}$ with edge-sharing BO_4 tetrahedra was synthesized under high-pressure (8 GPa) and high-temperature (1000 °C).[31] So far as we know, in tellurates, Te atoms commonly coordinate with six oxygen atoms forming TeO_6

octahedra, and TeO_6 octahedra are usually isolated or connected by sharing corner forming a three-dimension framework, hence tellurates with face sharing TeO_6 octahedra is very rare. Only $Ba_3Te_2O_9$ and $Ba_3Fe_2TeO_9$ exhibit face-sharing TeO_6 octahedra structures and $Ba_3Fe_2TeO_9$ shows face-sharing between Fe and Te, not totally two Te cations, while $K_3LaTe_2O_9$ is the first alkali-rare earth metal quaternary tellurate with face-sharing TeO_6 octahedra structure. Therefore, the discovery of $K_3LaTe_2O_9$ shows the potential of the lanthanide tellurates for displaying new types of crystal structure.

As mentioned above, structure of $K_3LaTe_2O_9$ is similar to that of $Ba_3Te_2O_9$ and $Ba_3Fe_2TeO_9$.[3, 12] The structure of $Ba_3Te_2O_9$ was determined by neutron power diffraction. It occurs in space group *P6₃/mmc* with unit cell parameters (a = 5.8603 Å, c = 14.3037 Å). Ba1, Ba2, Te1, O1, and O2 are in the Wyckoff sites 2d, 4f, 4e, 6h, and 12k, respectively, with 100% occupation of all atoms, and $[Te_2O_9]^{6-}$ anions are separated by Ba^{2+}, which are obviously different from the distributions of the cations in $K_3LaTe_2O_9$. As to $Ba_3Fe_2TeO_9$, the structure was solved and refined on the basis of neutron power diffraction data, which also belongs to space group *P6₃/mmc* with unit cell parameters (a = 5.767 Å, c = 14.1998 Å). $Ba_3Fe_2TeO_9$ is actually isostructural with $K_3LaTe_2O_9$, with K1, K2, La, and Te in latter compound corresponding to Ba1, Ba2, $M1$ ($M = Fe_{0.85}Te_{0.15}$) and $M2$ ($M = Fe_{0.57}Te_{0.43}$) in the former. Besides, $FeTeO_9$ groups in $Ba_3Fe_2TeO_9$ and Te_2O_9 groups in $K_3LaTe_2O_9$ are centrosymmetrical structures with mirror planes (Figure 5).

First-principles calculations

The first-principles studies were performed to further investigate the mechanism of the structural stability of the face-sharing $[Te_2O_9]^{6-}$ anion. As we known, vibrations in low frequency region are more likely to break up because they would shift to imaginary frequency region under external environment disturbance.[32] In $K_3LaTe_2O_9$ structure, related Te-O Raman spectra calculation results in low frequency around 200 cm^{-1} correspond to the vibration along the same direction of the $[Te_2O_9]$ group (as seen in Figure 10(a)). This kind of vibration would not cause the break of face-sharing $[Te_2O_9]$ group, thus the face-sharing $[Te_2O_9]^{6-}$ anion is stable to some extent. Figure 10 (b) exhibit the electronic density difference in the face-sharing $[Te_2O_9]$ groups, which shows a different charge redistribution among the face-sharing O(1) and cornersharing O(2). In detail, O(2) atoms obtain more electronic charges from the neighboring Te atoms, which indicates migration of electronic charges from Te-O(1) to Te-O(2) bond due to the modification of the chemical environment around the oxygen atoms as they are changed from face-sharing to corner-sharing. More quantitative results from the Mulliken analysis reveals that Te-O(1) and Te-O(2) Mulliken populations are 0.44 and 0.62, respectively. This implies that the corner-sharing oxygen atoms are more stable than the face-sharing oxygen atoms, consistent with the Pauling's second rule (i.e., the oxygen anion having more charge tends to be more stable).

Experimental band gap

Figure 6 shows the diffuse reflectance spectrum of $K_3LaTe_2O_9$. The absorption edge of $K_3LaTe_2O_9$ is 287 nm, from which a band gap of 4.32 eV is deduced.[33]

Thermal analysis

As shown in Fig. 7(a), TGA curve of $K_3LaTe_2O_9$ exhibits continue weight loss during the heating process and complete decomposition at 979 ℃. DSC heating curve (Figure 7(b)) of $K_3LaTe_2O_9$ exhibits two sharp endothermic peak at 755 ℃ and 845 ℃, respectively, which also indicates that it decomposes during heating. Therefore, single crystals of $K_3LaTe_2O_9$ must be grown by the flux method below the decomposition temperature.

Variable-temperature X-ray powder diffraction (VT-XRD)

To further investigate thermal properties of $K_3LaTe_2O_9$, variable-temperature X-ray powder diffraction was performed. As seen in Figure 8, impurity peaks appeared when temperature increasing. The main component of polycrystalline sample at 923 K is $K_3LaTe_2O_9$, with the impurity peaks corresponding to La_2TeO_6. The $K_3LaTe_2O_9$ had decomposed completely to La_2TeO_6 by 1023 K.

IR and Raman Spectra

Figure 9 shows the IR spectrum in the region of 400 cm^{-1} to 1200 cm^{-1}, and Raman spectrum between 100 cm^{-1} and 1200 cm^{-1}, by which it is difficult to confirm completely the coordination of Te atoms due to their complexity. It can be roughly inferred that the bands from 600-800 cm^{-1} (729 cm^{-1} and 768 cm^{-1}) correspond to the Te-O(2) stretching mode. Infrared vibration (565 cm^{-1}) observed in the 500-600 cm^{-1} region is assigned to Te-O(1) stretching mode. The bands in the low frequency region can be attributed to bending and deformation modes of the group.[12, 34]

Conclusions

A new quaternary alkali-lanthanide metal tellurate $K_3LaTe_2O_9$ has been grown as single crystals from a flux, which belongs to hexagonal space group *P6₃/mmc*. In the structure, $[Te_2O_9]^{6-}$ contains rare face-sharing TeO_6 octahedra, which are connected by LaO_6 octahedra and form a three dimensional framework structure. The VT-XRD results and the thermal analysis show that $K_3LaTe_2O_9$ decompose at high temperature. The first-principles calculations demonstrate the stability of the $[Te_2O_9]$ group, while the calculated electronic density difference and Mulliken population reveal that in $[Te_2O_9]$ group the corner-sharing oxygen atoms are more stable than the face-sharing oxygen atoms.

Acknowledgements

This work was supported by the National Natural Science Foundation of China (Grant Nos. 91422303 and 11174297) and China “863” project (No. 2015AA034203).

References

1. J. Yeon, S. H. Kim, S. D. Nguyen, H. Lee, P. S. Halasyamani, *Inorganic Chemistry.* 2012, 51, 2662.

2. R. Mathieu, S. A. Ivanov, R. Tellgren, P. Nordblad, *Physical Review B*, 2011, 83, 174420.

3. M. S. Augsburger, M. C. Viola, J. C. Pedregosa, R. E. Carbonio, J. A. Alonso, *Journal of Materials Chemistry*, 2006, 16, 4235.

4. M. Sathiya, K. Ramesha, G. Rousse, D. Foix, D. Gonbeau, K. Guruprakash, A. S. Prakash, M. L. Doublete, J. M. Tarascona, *ChemComm*, 2013,49, 11376.

5. J. Choisnet, A. Rulmont, P. Tarte, *Journal of Solid State Chemistry*, 1989, 82, 272.

6. V. B. Nalbandyan, M. Avdeev, M. A. Evstigneeva, *Journal of Solid State Chemistry*, 2013, 199, 62.

7. Y. S. Hong, M. Zakhour, M. A. Subramanian, J. Darriet, *Journal of Materials Chemistry*, 1998, 8, 1889.

8. M. Liegeois-Duyckaerts, *Spectrochimica Acta Part A: Molecular Spectroscopy*, 1985, 41, 523.

9. W. S. Zhang, H. J. Seo, *Journal of Alloys and Compounds*, 2013, 553, 183.

10. M. Kunz, I.D. Brown, *Journal of Solid State Chemistry*, 1995, 115, 395.

11. (a) M. L. López, M. L. Veiga, C. Pico, *Journal of Materials Chemistry*, 1994, 4, 547. (b) M. C. Knapp, P. M. Woodward, *Journal of Solid State Chemistry*, 2006, 179, 1076. (c) M. L. López, I. Alvarez, M. Gaitán, A. Jerez, C. Pico, M.L. Veiga, *Solid State Ionics*, 1993, 63, 599.

12. A. J. Jacobson, J. C. Scanlon, K. R. Poeppelmeier, J. M. Longo, *Materials Research Bulletin*, 1981, 16, 359.

13. Rigaku (2008). CrystalClear. Rigaku Corporation, Tokyo, Japan.

14. G. M. Sheldrick, *Acta Crystallogr., Sect. A: Found. Crystallogr.*, 2008, 64, 112.

15. L. M. Gelato, E. Parthé, *Journal of Applied Crystallography*, 1987, 20, 139.

16. R. S. Mulliken, *Journal of Physical Chemistry*, 1955, 23, 1833.

17. M. C. Payne, M. P. Teter, D. C. Allan, T. A. Arias and T. A. J. D. Joannopoulos, *Reviews of Modern Physics*, 1992, 64, 1045.

18. S. J. Clark, M. D. Segall, C. J. Pickard, P. J. Hasnip, M. J. Probert, K. Refson and M. C. Payne, *Zeitschrift für Kristallographie - Crystalline Materials*, 2005, 220, 567.

19. W. Kohn and L. J. Sham, *Physical Review*, 1965, 140, 1133

20. (a) J. P. Perdew, A. Zunger, *Physical Review B*, 1981, 23, 5048; (b) D. M. Ceperley, B. J. Alder, *Physical Review Letters*, 1980, 45, 566.

21. J. S. Lin, A. Qteish, M.C. Payne, V. Heine, *Physical Review B*, 1993, 47, 4174.

22. L. Kleinman, D.M. Bylander, *Physical Review Letters*, 1982, 48 1425.

23. H. J. Monkhorst, J. D.Pack, *Physical Review B*. 1976, 13, 5188.

24. W. Klein, J. Curda, E-M. Peters. M. Jansen, *Zeitschrift für Anorganische und Allgemeine Chemie*, 2005, 631, 2893.

25. L. Pauling, *Journal of the American Chemical Society*, 1929, 51, 1010.

26. J. K. Burdett, T. J. McLarnan, *American Mineralogist*, 1984, 69, 601.

27. C. T. Chen, T. Sasaki, R. K. Li, Y. C. Wu, Z. S. Lin, Y. Mori, Z. G. Hu, J. Y. Wang, G. Aka and M. Yoshimura, *Nonlinear Optical Borate Crystals, Wiley- VCH*, 2012

28. (a) C. Meade, R. J. Hemley and H. K. Mao, *Physical Review Letters*, 1992, 63, 1387; (b) M. Grimsditch, *Physical Review Letters*, 1984, 52, 2379; (c) R. M. Hazen, L. W. Finger, R. J. Hemley and H. K. Mao, *Solid State Communications*, 1989, 72, 507.

29. (a) A. K. Cheetham, G. Ferey and T. Loiseau, *Angewandte Chemie International Edition*, 1999, 38, 3268; (b) M. Estermann, L. B. Mccusker, C. Baerlocher, A. Merrouche and H. Kesler, *Nature*, 1991, 352, 320; (c) P. Y. Feng, X. H. Bu, S. H. Tolbert and G. D. Stucky, *Journal of the American Chemical Society*, 1997, 119, 2497;

(d) R. K. Brow, R. J. Kirkpatrick and G. L. Turner, *Journal of the American Chemical Society*, 1993, 76, 919.

30. (a) B. Stöger, M. Weil, E. Zobetz, *Zeitschrift für Kristallographie - Crystalline Materials*, 2010, 225, 125.; (b) P. Höss und T. Schleid, *Zeitschrift für Anorganische und Allgemeine Chemie*, 2007, 633, 1391.

31. (a) H. Huppertz and B. von der Eltz, *Journal of the American Chemical Society*, 2002, 124, 9376; (b) H. Huppertz and W. Schnick, *Chemistry- A European Journal*, 1997, 3, 249.

32. L. Yang, W. L. Fan, Y. L. Li, H. G. Sun, L. Wei, X. F. Cheng, X. Zhao, *Inorganic Chemistry*, 2012, 51, 6762.

33. O. Schevciw and W. B. White, *Materials Research Bulletin*, 1983, 18, 1059.

34. R. L. Frost, E. C. Keeffe, *Journal of Raman Spectroscopy*, 2009, 40, 249.

Figure Captions

Figure 1 Calculated and experimental X-ray diffraction patterns of $K_3LaTe_2O_9$.

Figure 2 Crystal structure of $K_3LaTe_2O_9$.

Figure 3 Coordination environments of the cations in $K_3LaTe_2O_9$.

Figure 4 Framework diagram of $K_3LaTe_2O_9$.

Figure 5 Te_2O_9 groups and $FeTeO_9$ groups in $K_3LaTe_2O_9$ (a) and $Ba_3Fe_2TeO_9$ (b).

Figure 6 Diffuse reflectance spectrum of $K_3LaTe_2O_9$.

Figure 7 TGA and DSC pattern of $K_3LaTe_2O_9$.

Figure 8 Variable-temperature X-ray powder diffraction patterns from 298 K to 1123 K.

Figure 9 Experimental IR and Raman spectrum.

Figure 10 Contour plots of the electronic density difference on the planes formed by Te and face-sharing O. The off-plane and O atoms are represented by small red balls.

Figure 1

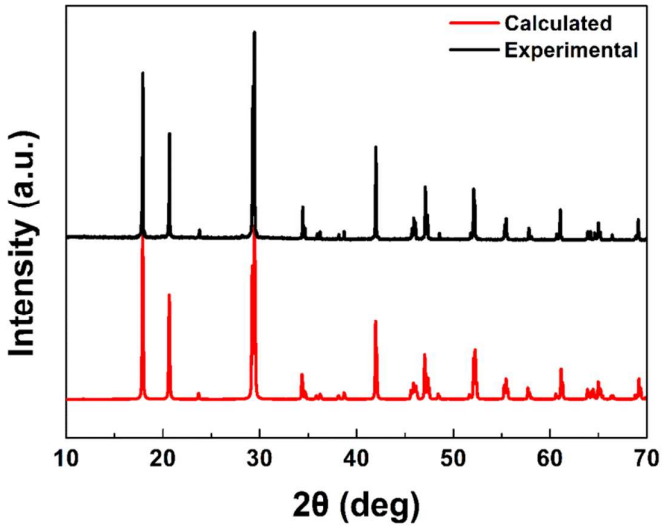
Calculated
Experimental
Intensity (a.u.)
10
20
30
40
50
60
70
2θ (deg)

Figure 2

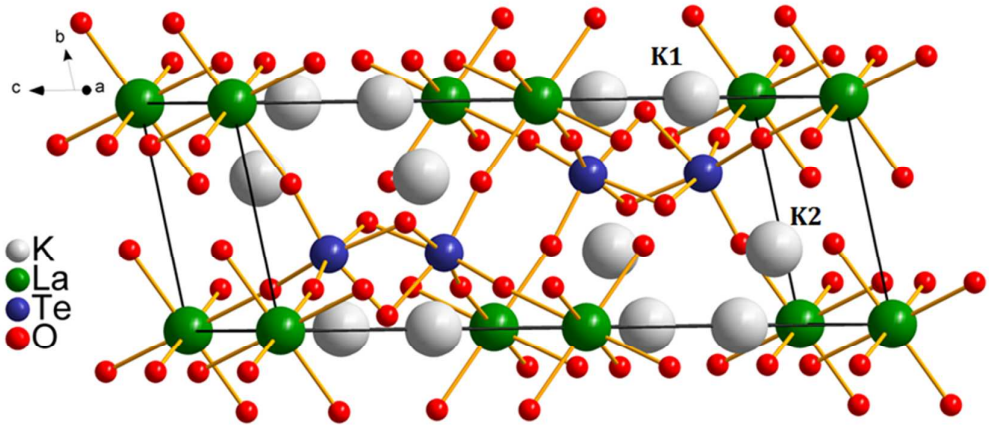

Figure 3

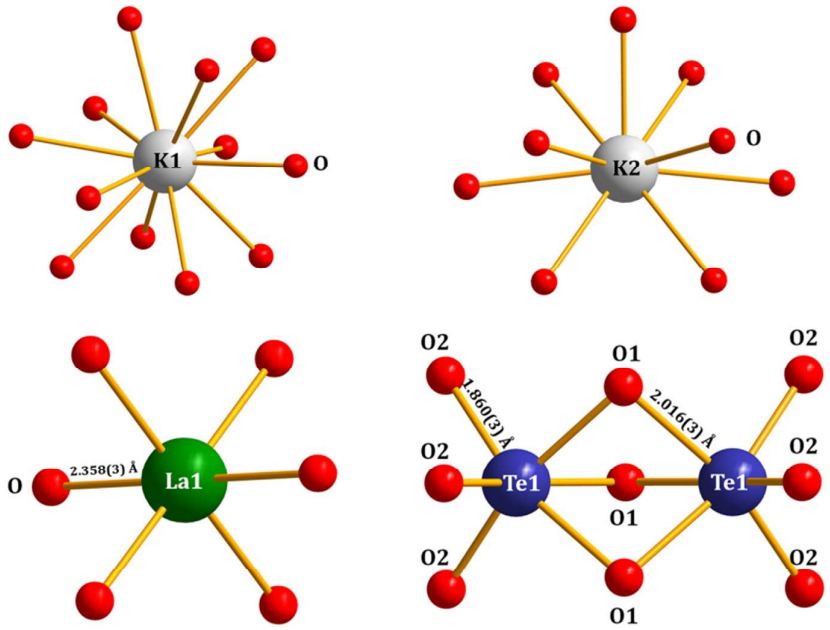
K1
O
K2
O
O
2.358(3) Å
La1
O2
1.860(3) Å
O1
2.016(3) Å
O2
O2
Te1
O1
Te1
O2
O2
O2
O1

Figure 4

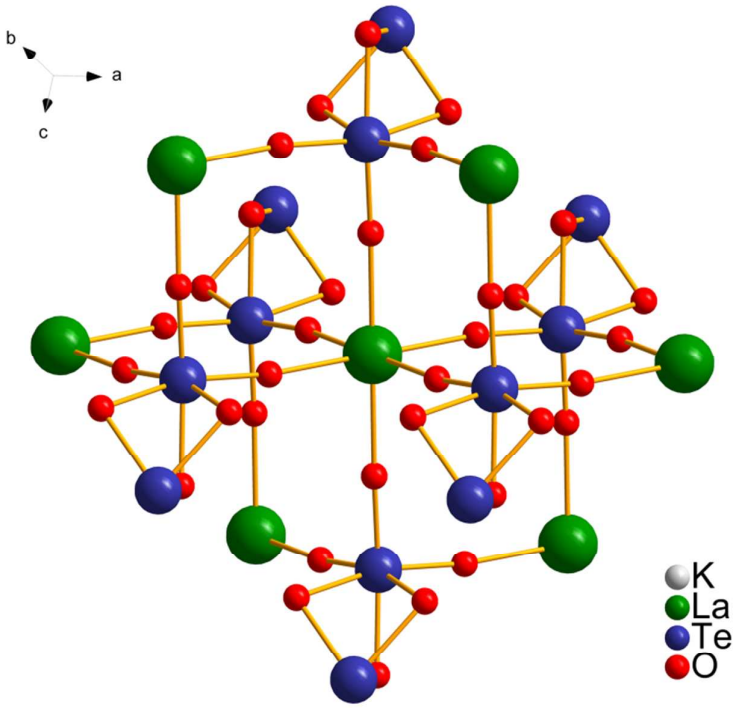

Figure 5

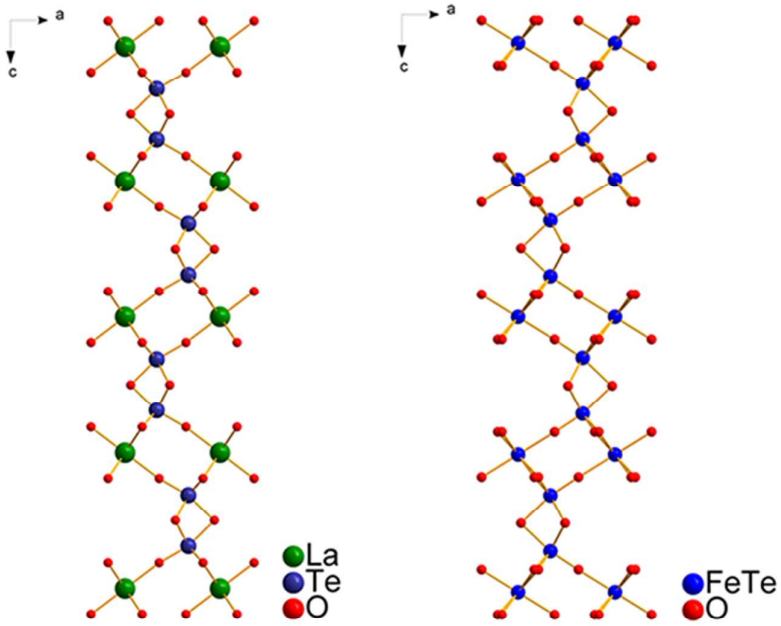

(a) (b)

Figure 6

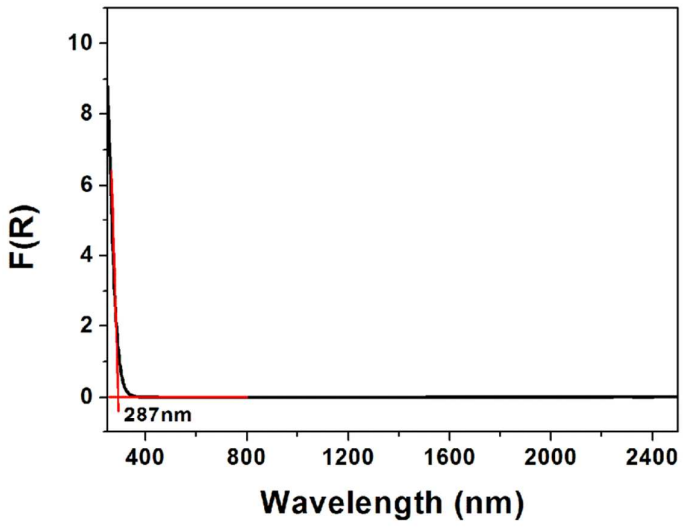

Figure 7

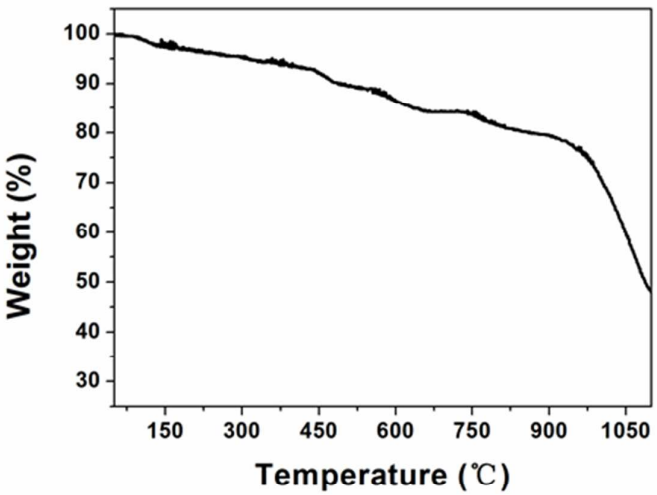
Weight (%)
100
90
80
70
60
50
40
30
150
300
450
600
750
900
1050
Temperature (℃)

(a)

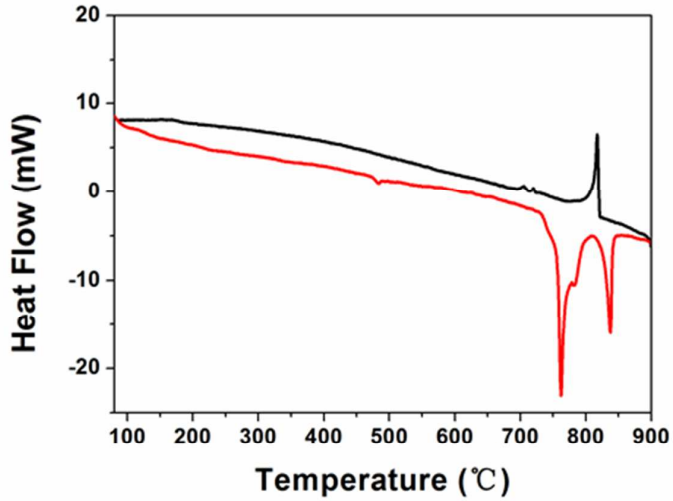
Heat Flow (mW)
20
10
0
-10
-20
100
200
300
400
500
600
700
800
900
Temperature (℃)

(b)

Figure 8

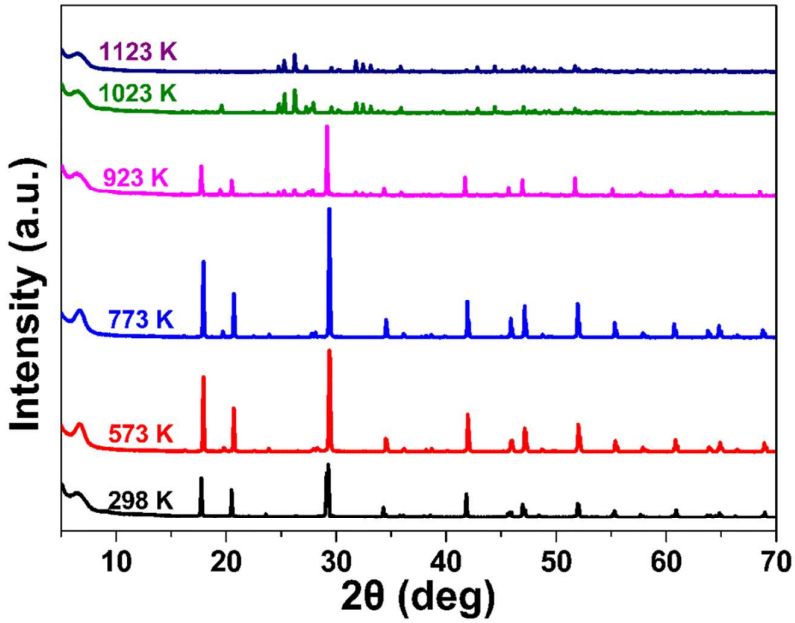
1123 K
1023 K
923 K
773 K
573 K
298 K
Intensity (a.u.)
10
20
30
40
50
60
70
2θ (deg)

Figure 9

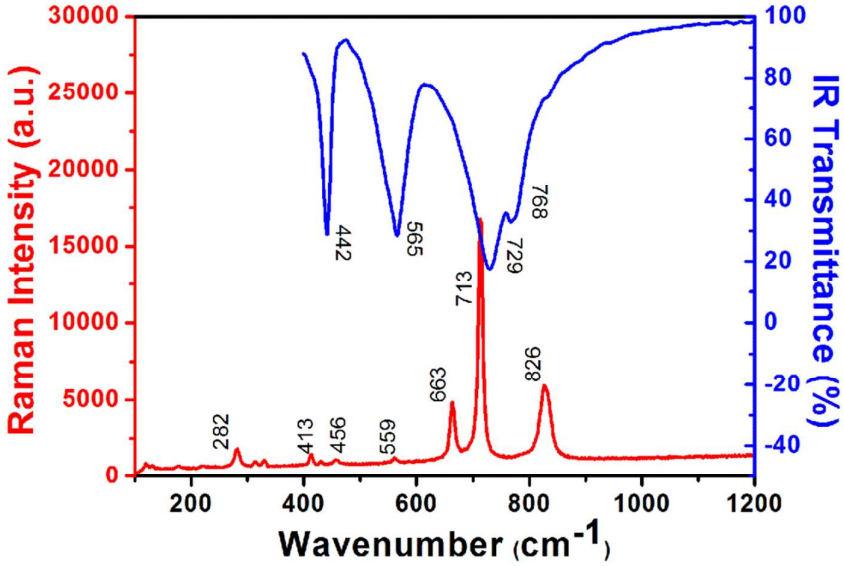
Raman Intensity (a.u.)
IR Transmittance (%)
Wavenumber (cm-1)
30000
25000
20000
15000
10000
5000
0
100
80
60
40
20
0
-20
-40
200
400
600
800
1000
1200
282
413
456
559
663
713
826
442
565
729
768

Figure 10

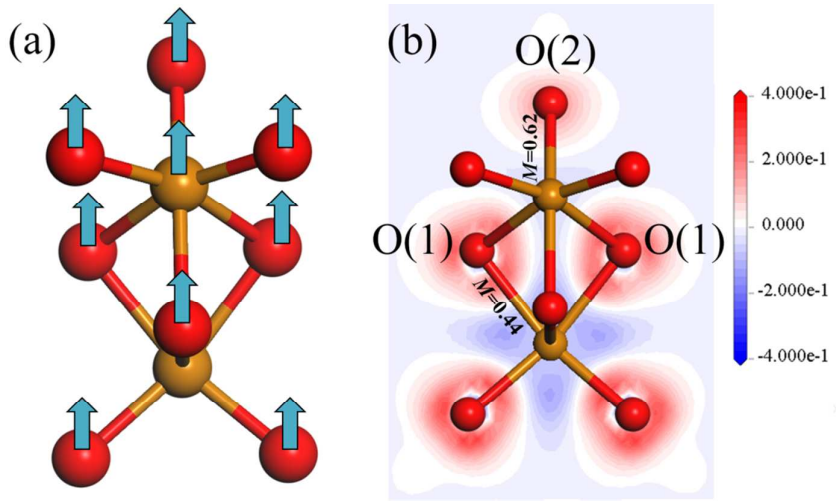

Table 1. Crystal data and structure refinements for $K_3LaTe_2O_9$

	$K_3LaTe_2O_9$
Fw	655.41
Crystal system	Hexagonal
Space group	*P6₃/mmc*
a(Å)	6.0589(9)
c(Å)	15.024(3)
V(Å^3)	477.6(1)
Z	2
T(K)	153
Λ(Å)	0.71073
ρ_c(g/cm3)	4.557
μ(cm^{-1})	11.792
R_{int}	0.0377
R(F)[a]	0.0227
R_w(Fo^2)[b]	0.0465

[a] $R(F) = \sum | \, | F_o | - | F_c | \, | / \sum | F_o |$ for $F_o^2 > 2\sigma(F_o^2)$.

[b] $R_w(F_o^2) = \{\sum [w(F_o^2 - F_c^2)^2] / \sum w F_o^4\}^{1/2}$ for all data. $w^{-1} = \sigma^2(F_o^2) + (zP)^2$, where $P = (\mathrm{Max}(F_o^2, 0) + 2 F_c^2)/3$; $z = 0.02$.

Table 2. Selected bond lengths(Å) and bond angles(°) for $K_3LaTe_2O_9$

K1—O2×7	3.000(3)	K2—O2×3	3.0505(18)
K1—O1×6	3.0454(6)	La1—O2×7	2.358(3)
K1—O1	3.0505(18)	Te1—O2×3	1.860(3)
K2—O1×4	2.875(3)	Te1—O1×4	2.016(3)
K2—O2×5	3.0504(6)	O2—Te1—O2×3	97.52(12)
O2—La1—O2×6	87.49(10)	O2—Te1—O1×6	92.18(9)
O2—La1—O2×6	92.51(10)	O2—Te1—O1×3	165.24(12)
O2—La1—O2vi×3	180.0(1)	O1—Te1—O1×3	76.29(12)
Te1—O1—Te1	89.00(15)	Te1—O2—La1	172.71(16)

Table 3. Atomic coordinates, equivalent isotropic displacement parameters (Å^2), and calculated bond valence sum (BVS) for $K_3LaTe_2O_9$.

Atom	Wyck.	Site	x/a	y/b	z/c	U_{eq} (Å^2)[a]	BVS
K1	2b	-6m2	0	0	3/4	0.0086(4)	1.086
K2	4f	3m.	1/3	2/3	0.61656(11)	0.0122(3)	0.909
La1	2a	-3m.	0	0	1/2	0.00297(16)	3.414
Te1	4f	3m.	-1/3	1/3	0.65593(3)	0.00287(15)	5.784
O1	6h	mm2	-0.0592(7)	0.4704(4)	3/4	0.0049(7)	1.964
O2	12k	.m.	-0.6412(5)	0.1794(2)	0.5945(2)	0.0088(6)	1.916

[a] U_{eq} is defined as one-third of the trace of the orthogonalized U_{ij} tensor.